Electronic Supplementary Material (ESI) for Materials Chemistry Frontiers.

Supplementary Information (SI)

The alumination mechanism of porous silica materials and properties of derived ion exchangers and acid catalysts

Zheng Li,[a] Michael Benz,[a] Carolin Rieg,[a] Daniel Dittmann,[a] Ann-Katrin Beurer,[a] Dorothea Häussermann,[a] Bjørnar Arstad,[b] and Michael Dyballa[a]*

[a] Institute of Technical Chemistry, University of Stuttgart, Pfaffenwaldring 55, 70569 Stuttgart, Germany

[b] SINTEF Industry, Forskningsveien 1, 0373 Oslo, Norway

*Corresponding author, E-mail: michael.dyballa@itc.uni-stuttgart.de

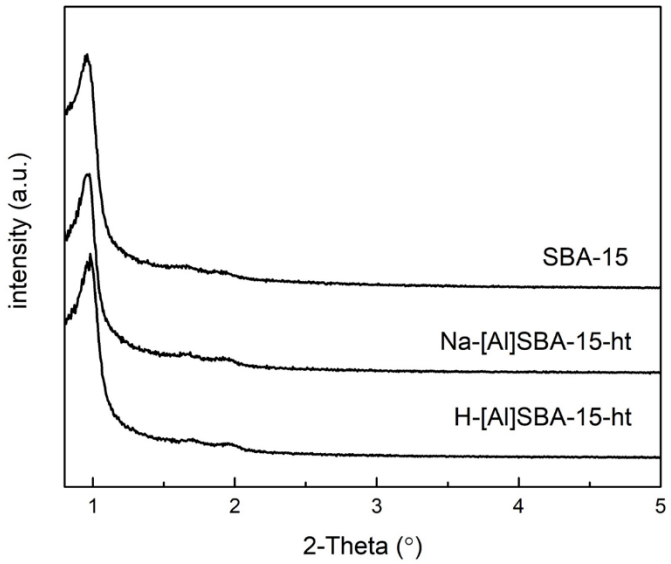

Figure S1. Small-angle X-ray powder diffraction patterns of the mesoporous SBA-15 materials under study.

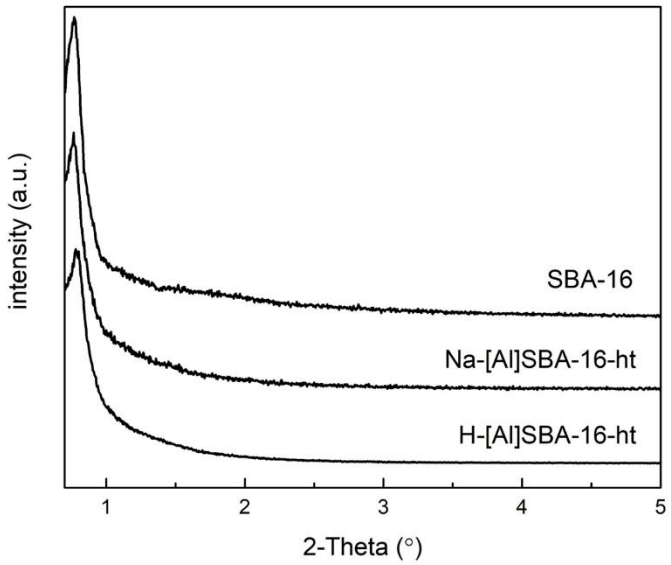

Figure S2. Small-angle X-ray powder diffraction patterns of the mesoporous SBA-16 materials under study.

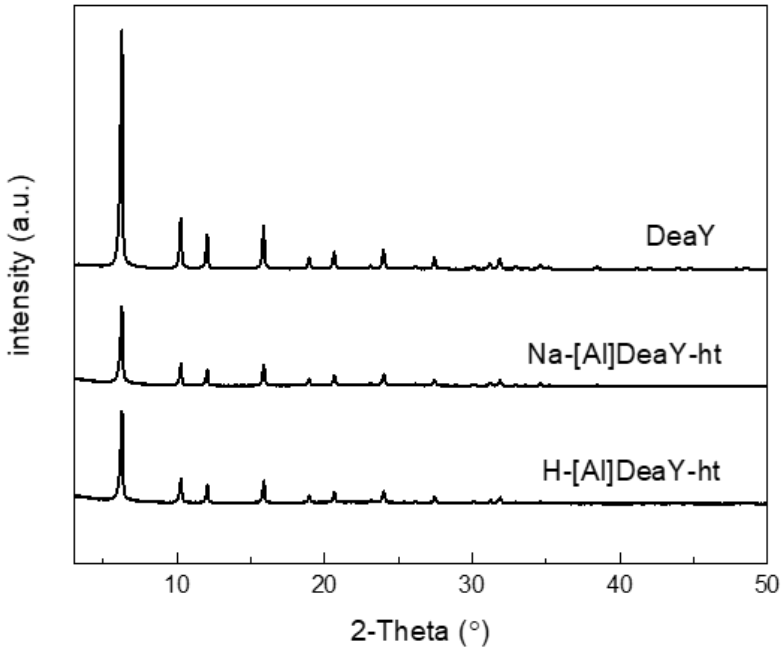

Figure S3. Wide-angle X-ray powder diffraction patterns of the microporous DeA-Y zeolites under study.

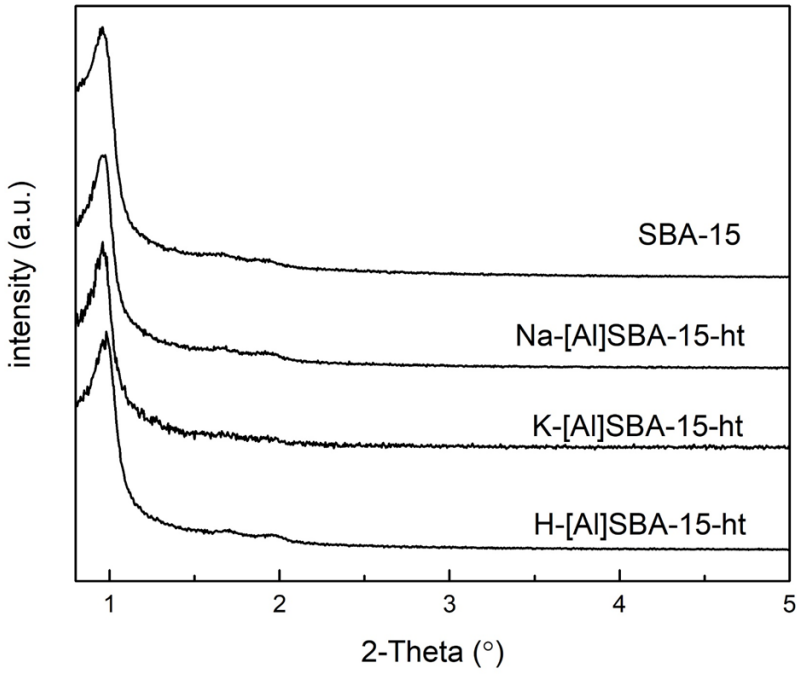

Figure S4. Small-angle X-ray powder diffraction patterns of ion exchanged forms of mesoporous [Al]SBA-15-ht under study.

Table S1: Si/Al ratio of synthesis batch (raw) and of modified materials (modified).

Product	m(Substrate) [g]	m($NaAlO_2$) [g]	Si/Al (raw)	Si/Al (modified)
Na-[Al]SBA-15-low	3	0.15	27	29
Na-[Al]SBA-15-high	1	0.12	11	13
Na-[Al]SBA-15-ht	1	0.12	11	12
Na-[Al]SBA-16-low	2.2	0.13	23	29
Na-[Al]SBA-16-high	2.2	0.26	11	20
Na-[Al]SBA-16-ht	2.2	0.26	11	12
Na-[Al]DeaY-ht	2.2	0.26	11	21

Table S2: Pore diameters of SBA-15 determined by the BJH-method on the adsorption (left) and desorption (right) branch.

Material	Mesopore diameter [nm]^{ads}	Mesopore diameter [nm]^{des}
SBA-15	6.8	5.7
Na-[Al]SBA-15-low	6.7	5.4
H-[Al]SBA-15-low	6.6	5.4
Na-[Al]SBA-15-high	6.7	5.5
H-[Al]SBA-15-high	6.7	5.4
Na-[Al]SBA-15-ht	6.7	5.4
H-[Al]SBA-15-ht	6.7	5.5

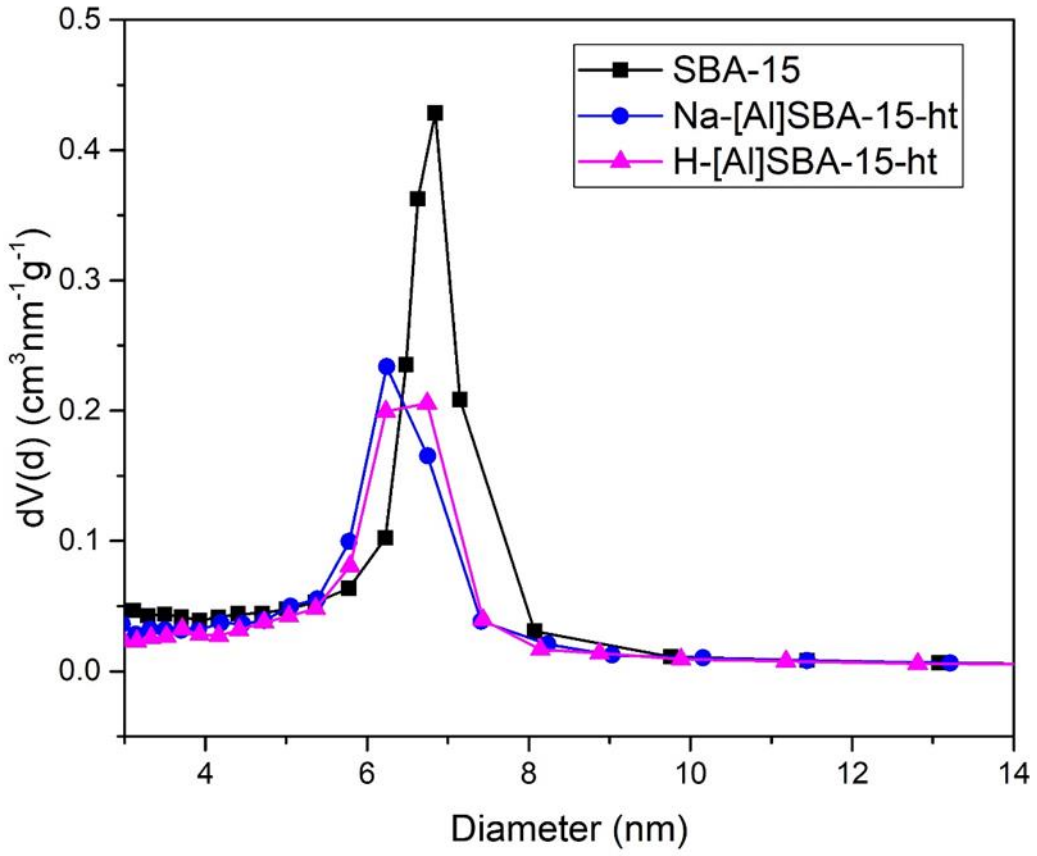

Figure S5: Pore size distribution according to the BJH method for SBA-15, Na-[Al]SBA-15-ht, and H-[Al]SBA-15-ht (adsorption branch).

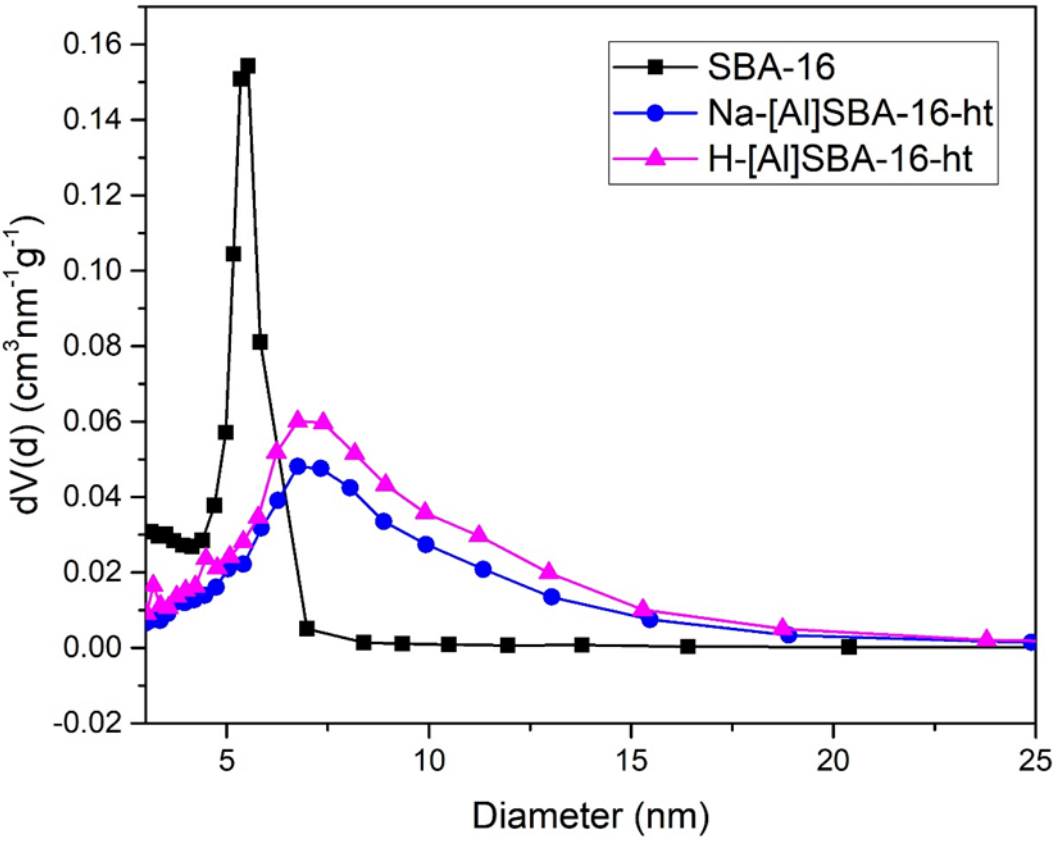

Figure S6: Pore size distribution according to the BJH method for SBA-16, Na-[Al]SBA-16-ht, and H-[Al]SBA-16-ht.

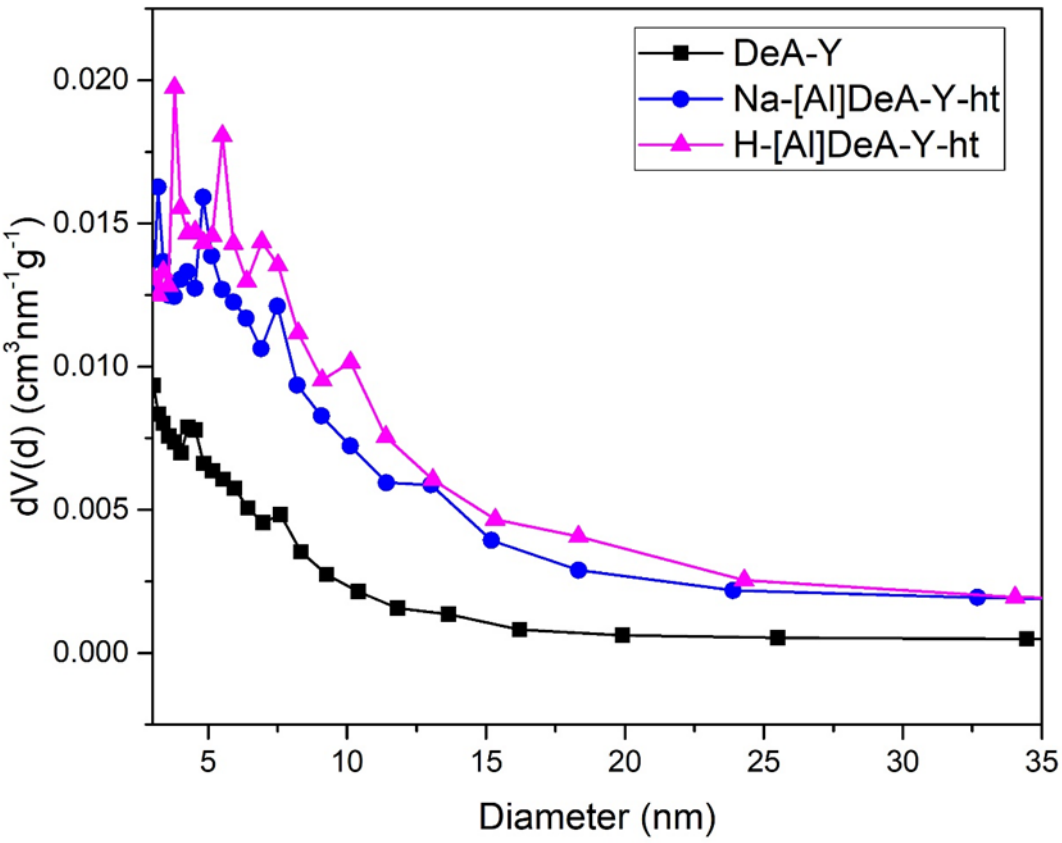

Figure S7: Pore size distribution according to the BJH method for DeA-Y, Na-[Al]DeA-Y-ht, and H-[Al]DeA-Y -ht.

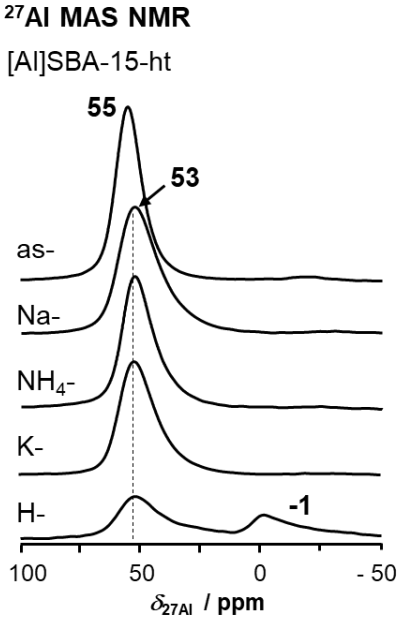

Figure S8. ^{27}Al MAS NMR spectra of the as-, Na-, NH_4-, K-, and H-forms of material [Al]SBA-15-ht.

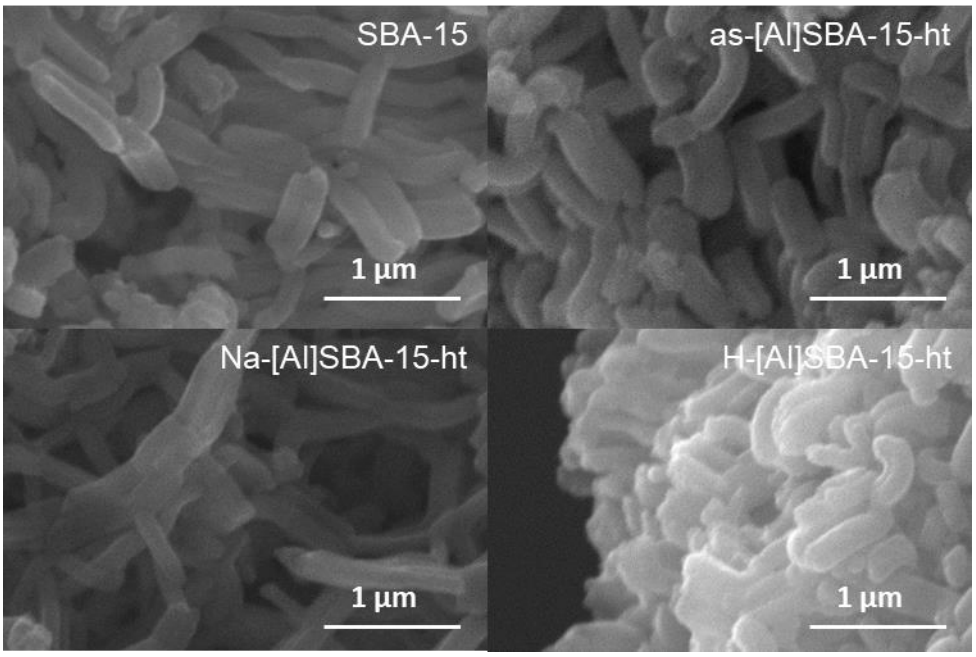

Figure S9: SEM pictures of all mesoporous SBA-15 forms.

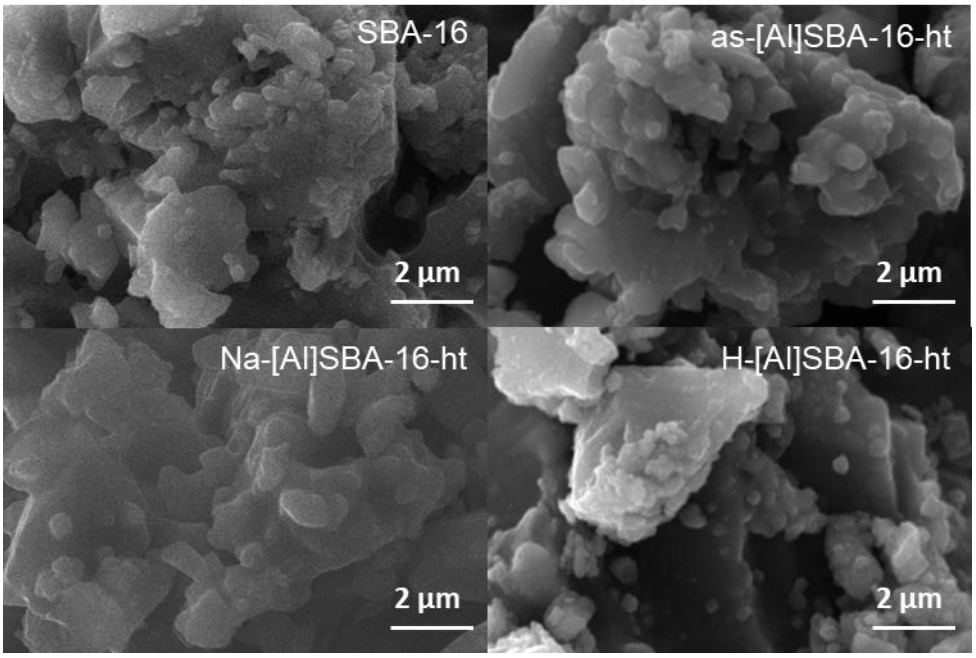

Figure S10: SEM pictures of all mesoporous SBA-16 forms.

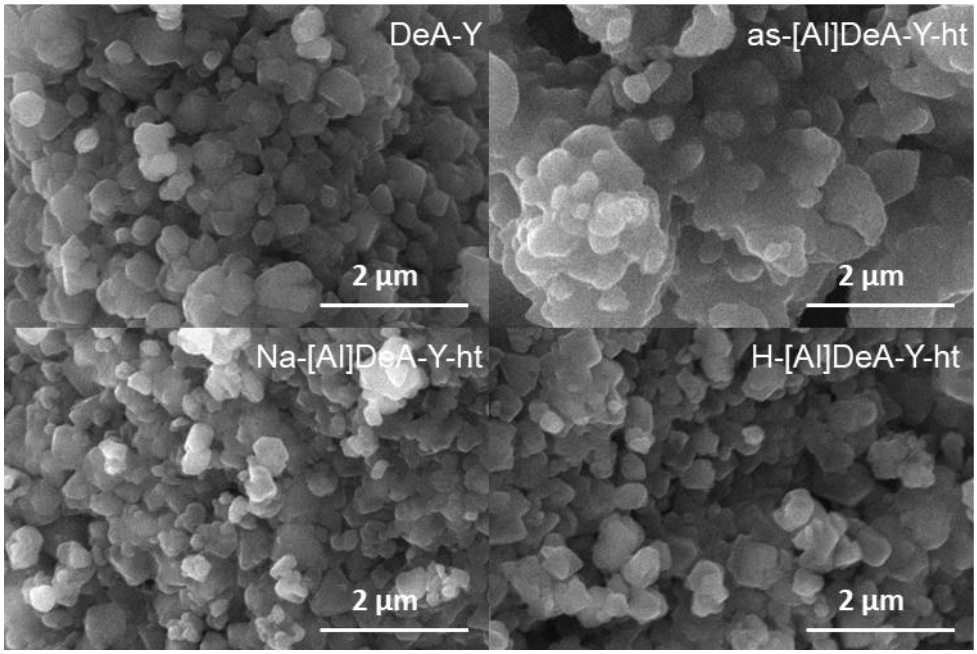

Figure S11: SEM pictures of all microporous DeA-Y forms.

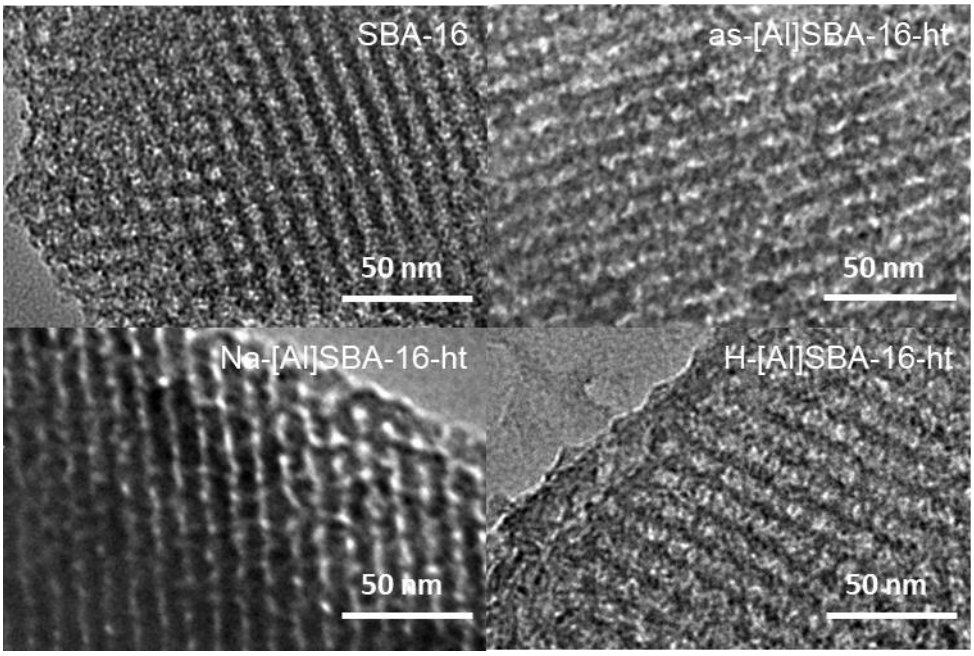

Figure S12: TEM-pictures of mesoporous SBA-16 in all steps of the synthesis procedure.

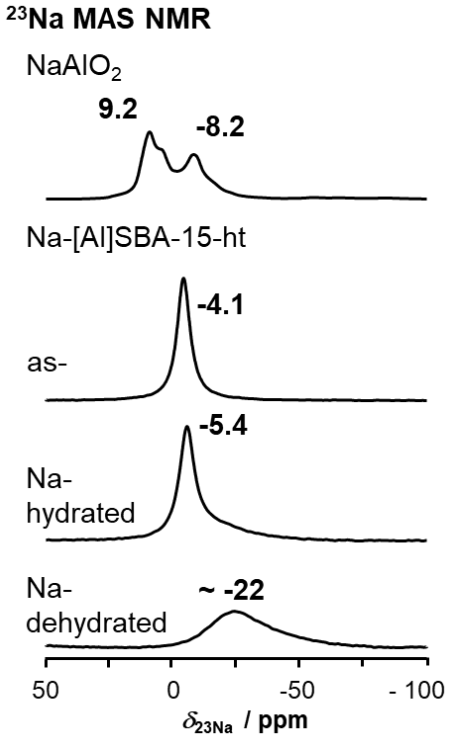

Figure S13. ^{23}Na MAS NMR spectra of the precursor $NaAlO_2$ and of fully hydrated Na-[Al]SBA-15-ht.

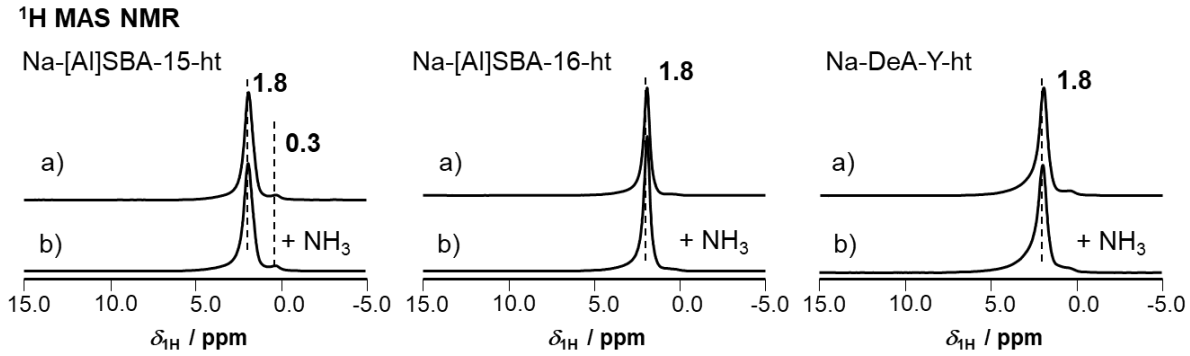

Figure S14: ^{1}H MAS NMR spectra before (a) and after (b) loadings with ammonia (NH_3) on activated Na-form materials. No peaks at 6.5 ppm due to the formation of NH_4^+ are observed and thus no Brønsted acid sites are present.

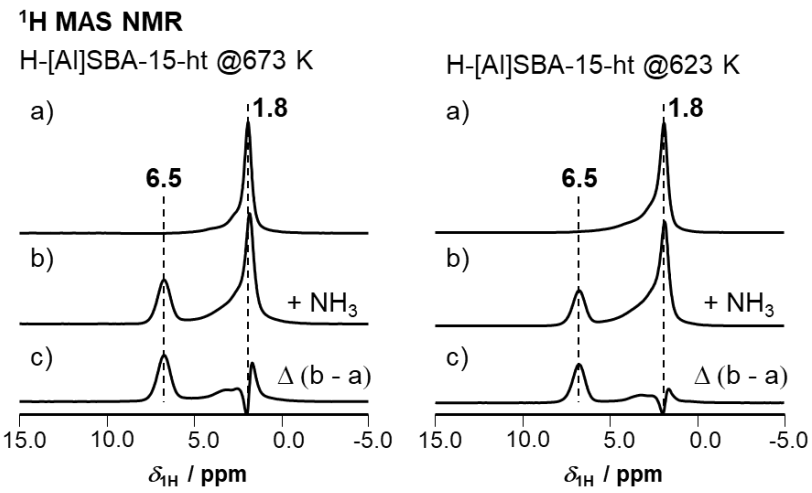

Figure S15: ^{1}H MAS NMR spectra (from top to bottom) before (a) and after (b) loadings with ammonia (NH_3) as well as the difference spectra (c). A comparison of materials with ammonia removal at different temperatures gave acid site densities of 0.12 mmol/g when the activation was performed under standard conditions in vacuum at 673 K and 0.10 mmol/g when the activation was performed in vacuum at 623 K.